Supporting Information

Copper-Based Metal-Organic Framework Overcomes Cancer Chemoresistance through Systemically Disrupting Dynamically balanced Cellular Redox Homeostasis

Jia Liu[1,#], Ye Yuan[1,2,#], Yanni Cheng[1], Daan Fu[1,2], Zhongyin Chen[1], Yang Wang[1], Lifang Zhang[1], Chundong Yao[1], Lin Shi[1], Mingyi Li[1], Cheng Zhou[1,2], Meizhen Zou[3], Guobin Wang[2,*], Lin Wang[1,3,*], Zheng Wang[1,2,*]

[1] Research Center for Tissue Engineering and Regenerative Medicine, Union Hospital, Tongji Medical College, Huazhong University of Science and Technology, Wuhan, 430022, China.

[2] Department of Gastrointestinal Surgery, Union Hospital, Tongji Medical College, Huazhong University of Science and Technology, Wuhan, 430022, China.

[3] Department of Clinical Laboratory, Union Hospital, Tongji Medical College, Huazhong University of Science and Technology, Wuhan, 430022, China.

Contents

Materials and methods

Materials

Cu $(NO_3)_2 \cdot 3H_2O$, dimethyl sulfoxide (DMSO), hydrochloric acid (HCl), methanol and nitric acid (HNO_3) were purchased from Sinopharm chemical regent Co., Ltd (Shanghai, China). Tris Base was obtained from GBCBIO Technologies Inc. 2,3,6,7,10,11-hexahydroxytriphenylene (HPT) was purchased from Shanghai Dibo Biotechnology Co., Ltd. Glutathione (GSH) and Glutathione reduced ethyl ester (GSH-OEt) was obtained from Aladdin Industrial Corporation (Shanghai, China).

Synthesis of CuHPT

Cu $(NO_3)_2 \cdot 3H_2O$ and HPT were dissolved in deionized water (10 mM) and DMSO (10 mM), respectively. Then, HPT solution (2 mL) was added dropwise into $Cu(NO_3)_2 \cdot 3H_2O$ aqueous solution (1 mL) and stirred for 10 min. Next, the pH value of solution was adjusted by tris solution (20 mM, pH 8.0) to 7.4, and the solution was stirred at room temperature for 1 h. The CuHPT was collected by centrifugation, and washed with methanol and water for three times, then dried by vacuum.

Characterization

Nano-ZS ZEN3600 (Malvern) was used to determine the size and zeta potential of CuHPT. The morphology was observed by a transmission electron microscope (Hitachi HT7800) and high-resolution transition electron microscopy (HR-TEM) was performed on FEI TALOS 200X. XRD pattern of CuHPT was performed on Quantum-IPlus 400 spectrometer (Zhongke-Niujin, Wuhan). XPS spectra were obtained by ESCALAB 250Xi XPS (Thermo Fisher). The Cu content of CuHPT was determined to be 20.01% by ICP-AES (iCAP 7000 Series ICP Spectrometer).

Degradation of CuHPT by GSH

CuHPT (100 μg mL^{-1}) was dispersed in 50% DMSO aqueous solution containing different contents of GSH (0, 2, 5, 10, 20 mM), and incubated for 10 min at room temperature. Subsequently, the supernatants were obtained and measured by UV-Vis spectrophotometer (Lambda Bio40 UV/Vis spectrometer, Perkin–Elmer) at 449 nm.

GSH oxidation by CuHPT

CuHPT dispersion (1 mg mL^{-1}) was mixed with GSH (10 mM), and then shaken at room temperature. At different time points (10 min, 20 min, 30 min, 1 h, 2 h, 4 h, 8 h), the supernatants were collected and measured using GSH and GSSG Assay Kit (Beyotime biotechnology).

H_2O_2 generation assay

HPT and CuHPT were dispersed in PBS, respectively. The dispersions were shaken at room temperature for 24 h. After that, the supernatants were collected, and the H_2O_2 contents were measured using Hydrogen Peroxide Assay Kit (Beyotime biotechnology).

•OH generation assay

CuHPT (400 μg mL^{-1}) or Cu^{2+} (8 mM) was mixed with GSH (5, 10, 20, 40, 80 mM) and shaken at room temperature for 15 min. Then, the supernatants were mixed with coumarin (5 mM, Aladdin Industrial Corporation) and H_2O_2 (80 mM). The resulting solutions were measured by fluorospectrophotometer (LS55, PerkinElmer, Ex: 332 nm).

Cell culture and animal

Human colorectal carcinoma cells (HCT116), human breast cancer cells (MCF7), human ileocecal colorectal adenocarcinoma cells (HCT-8), and their corresponding drug-resistant cells (HCT116/L-OHP, MCF7/ADR, and HCT-8/TAX) were incubated in the media (DMEM or RPMI1640, Gibco) containing 10% fetal bovine serum (FBS, ScienCell), and supplemented with 100 units mL^{-1} penicillin and 100 μg mL^{-1} streptomycin. All the media was maintained at 37°C under 5% CO_2.

Female BALB/c nude mice (6 Weeks, 18~20 g) were purchased from Beijing Vital River Laboratory Animal Technology Co., Ltd., and female BALB/c mice (6 Weeks, 18~20 g) were purchased from SPF (Beijing) Biotechnology Co., Ltd.. All of the animal experiments were performed following the guideline approved by the Institution Animal Care and Use Committee (IACUC) at Tongji Medical College, Huazhong University of Science and Technology, Wuhan, China (IACUC Number: S2386).

In vitro antitumor effect of CuHPT

Three types of drug-resistant cancerous cell lines (HCT116/L-OHP, MCF7/ADR, and HCT-8/TAX) and their parental cancer cells (HCT116, MCF7, and HCT-8) were seeded in 96-well plates at a density of 6×10^3 cells per well and cultured for 24 h. After that, CuHPT (0 to 40 μg mL^{-1}), Cu^{2+} (0 to 8 μg mL^{-1} of Cu^{2+}) or HPT (0 to 28 μg mL^{-1}) were added and cultured with cells for another 48 h. Then, the cells were washed with PBS for three times. The cell viability was examined using CCK-8 (MedChemExpress) according to the manufacture's instruction. The cytotoxicity of chemotherapeutic agents (oxaliplatin, doxorubicin (DOX), and paclitaxel (PTX)) in the drug-resistant cancer cells and their parental cancer cells was also determined using CCK-8 assay.

To study the influence of intracellular GSH level on cytotoxicity of CuHPT, HCT116 cells were first cultured in 96-well plates (6×10^3 cells per well) for 24 h, and then incubated with GSH-OEt (5 mM) or NAC (0.4 mM) for 8 h. Subsequently, these cells were exposed to CuHPT for another 48 h. The cell viability was determined using CCK-8 assay.

For cellular apoptosis assay, the cancer cells were seeded in 6-well plates at a density of 10^6 cells per well and cultured for 24 h, and subsequently exposed to CuHPT (50 μg mL^{-1}) for another 24 h. Next, the cells were harvested, and stained with Annexin-V-FITC/PI apoptosis detection kit (SUNGENE BIOTECH Ltd.) according to the manufacturer's instructions, and assessed by flow cytometry (LSRFortessa X20 Flow Cytometry System, BD Bioscience).

For Live/dead cells staining analysis, the cells were stained with Calcein AM and Propidium Iodide (PI) (Beyotime biotechnology) and then imaged using Olympus IX73 microscope.

Intracellular GSH/GSSG detection

The drug-resistant cancer cells and their parent cells were seeded in 6-well plates at a density of 10^6 cells per well and cultured for 24 h, respectively. Then, the cells were collected and measured by GSH and GSSG Assay Kit. The total protein was examined by BCA Protein Assay Kit (Beyotime biotechnology).

To test the GSH oxidation by CuHPT, the cancer cells were cultured in 6-well plates (10^6 cells per well) for 24 h, subsequently exposed to CuHPT (10 or 20 μg mL^{-1}) for 24 h. Finally, the intracellular GSH and GSSG mass were measured.

Intracellular ROS detection

HCT116/L-OHP or HCT116 cells were cultured in 6-well plates (10^6 cells per well) for 24 h. Then, the cells were exposed to CuHPT (50 μg mL^{-1}) or HPT (20~40 μg mL^{-1}) for 24 h, and collected. To test the total ROS level, the cells were stained with DCFH-DA (Reactive Oxygen Species Assay Kit, Byotime biotechnology) and analyzed by flow cytometry. The major types of cellular ROS (H_2O_2, •OH, and $O_2^{\bullet-}$) were determined using Dihydroethidium (DHE, $O_2^{\bullet-}$, Byotime biotechnology), cell-based Hydrogen Peroxide Assay (H_2O_2, Abcam), aminophenyl fluorescein (APF, •OH) (Shanghai Maokang Biotechnology Co., Ltd.), and coumarin (•OH), respectively.

***In vivo* antitumor activity**

HCT116/L-OHP cells (1×10^7 cells) were subcutaneously inoculated in the right flank of BALB/c nude mice. The mice were randomly divided into three groups (n = 8) when the mean tumor volume reached 80 mm^3. Then, these mice were treated with PBS, oxaliplatin (5 mg kg^{-1}), and CuHPT (5 mg kg^{-1}) every three days for four times, respectively. The body weight, longest tumor dimension (L), and shortest tumor dimension (W) were recorded every two days. The tumor volume was calculated as: $V = L \times W^2/2$. The relative tumor volume was calculated as the ratio between the tumor volume at a given time and the tumor volume at the initial time of treatment. At 14 days after the first treatment, the mice were sacrificed and tumors were isolated.

***In vivo* ROS detection**

HCT116/L-OHP cells (1×10^7 cells) were subcutaneously inoculated in the right flank of BALB/c nude mice. The mice were randomly divided into three groups when the mean tumor volume reached 90 mm^3. Then, these mice were treated with PBS, oxaliplatin (5 mg kg^{-1}), and CuHPT (5 mg kg^{-1}). After 24 h, 20 μL of DCFH-DA solution (80 μM) was peritumorally injected into the mice. One h later, the mice were sacrificed and the tumors were isolated and frozen at -80 C°. The cryosections were observed by a fluorescence microscope.

Biosafety of CuHPT

Healthy female BALB/c mice were intravenously injected with PBS, oxaliplatin (5 mg kg^{-1}),

and CuHPT (5 mg kg^{-1}) every three days for four times, respectively. The body weight was recorded every two days. At day 10, the mice were sacrificed and major organs were obtained for hematoxylin and eosin staining. Meanwhile, the blood samples were collected for serum biochemical analysis.

Cu contents biodistribution and clearance

Female BALB/c mice were intravenously injected with CuHPT (5 mg kg^{-1}). At different time points (1 d, 7 d, and 14 d), mice were sacrificed and major organs were harvested (heart, liver, spleen, lung, and kidney). Then, the organs were digested by microwave digestion, and the Cu content was measured using atomic absorption spectrometry (iCE 3000, Thermo Scientific). The mice only received PBS were set as the start time point (0 day).

Statistical analysis

The significant difference was determined by student's t-test and one-way ANOVA. Log-rank (Mantel-Cox) test was used for survival analysis. Statistically significant differences were defined as follow: $*P < 0.05$, $**P < 0.01$, $***P<0.001$, N.S., not significant.

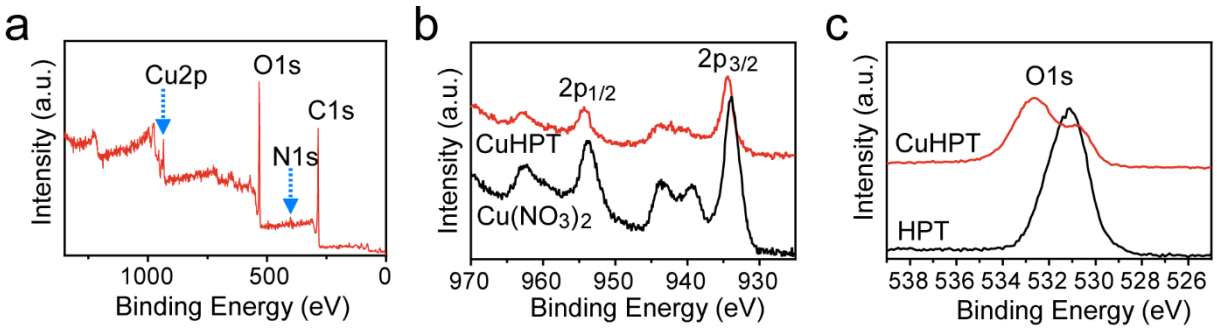

Figure S1. XPS spectra. (a) Full scan of CuHPT. (b) Cu 2p of CuHPT and $Cu(NO_3)_2$. (c) O 1s of CuHPT and HPT.

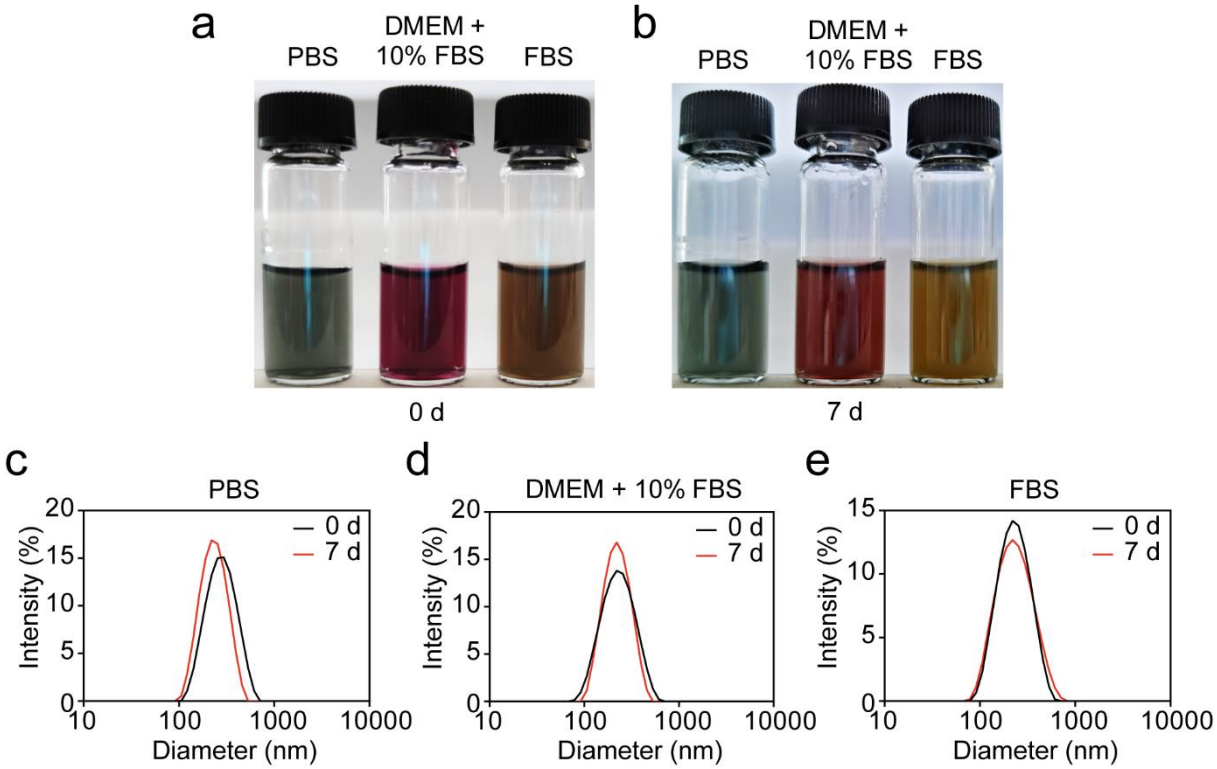

Figure S2. Stability of CuHPT. Images of CuHPT dispersed in PBS, DMEM + 10% FBS or FBS for 0 d (a) and 7 d (b). The size distributions of CuHPT dispersions in PBS (c), DMEM containing 10% FBS (d) and FBS (e) for 0 d and 7 d.

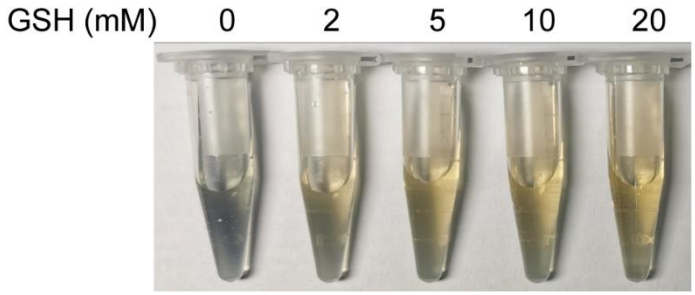

Figure S3. Image of CuHPT incubated with GSH for 10 min in DMSO aqueous solution (50%).

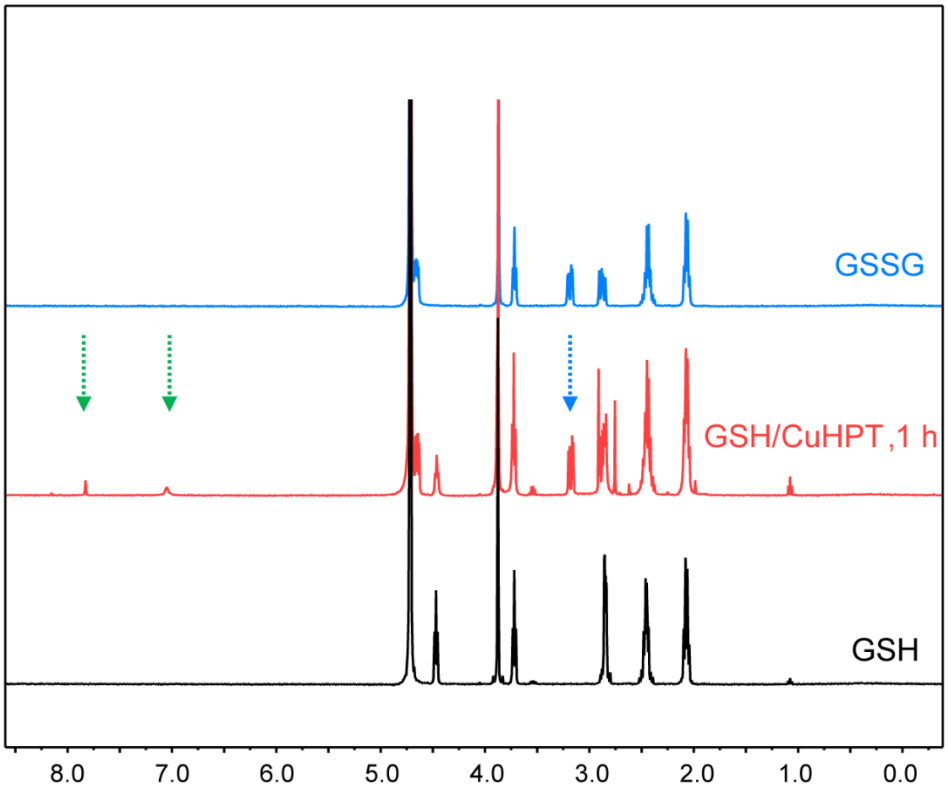

Figure S4. The ^{1}H NMR spectra of GSH, GSH/CuHPT, and GSSG in D_2O. The GSH was mixed with CuHPT for 1 h at room temperature, and the supernatant was characterized by NMR. The blue arrow indicates characteristic peak of GSSG, and the green arrows indicate characteristic peaks of HPT.

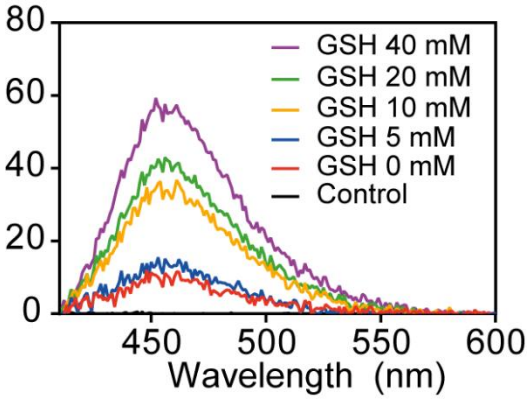

Figure S5. •OH generation of Cu^{2+} in the presence of GSH.

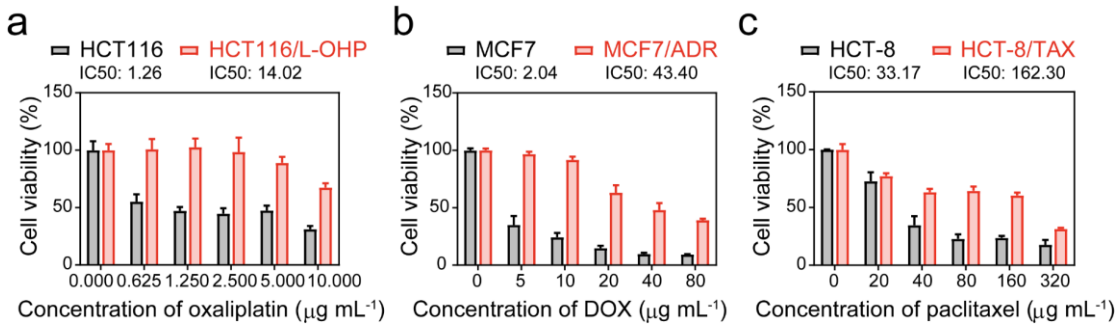

Figure S6. The cytotoxicity (IC50 values, μg mL^{-1}) of chemotherapeutic drugs in drug-resistant cancer cells and their drug-sensitive parental cancer cells.

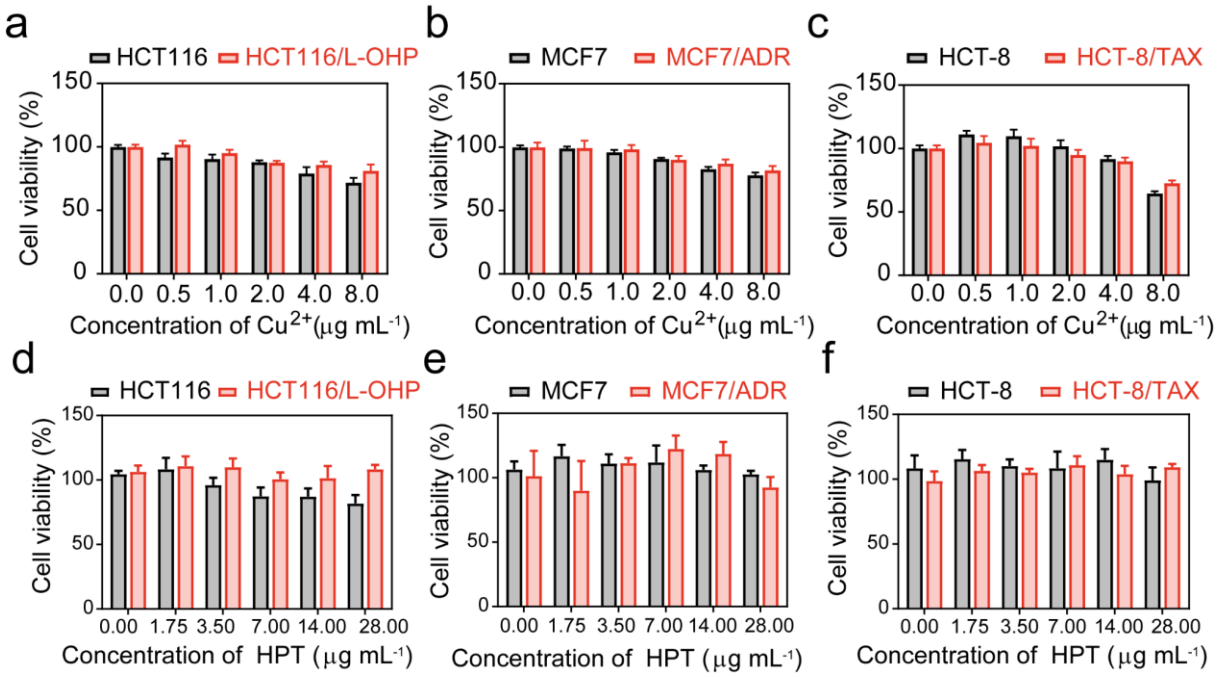

Figure S7. *In vitro* antitumor effects of Cu^{2+} and HPT. (a-c) Viability of HCT116 and HCT116/L-OHP (a), MCF7 and MCF7/ADR (b), HCT-8 and HCT-8/TAX (c) cells treated with Cu^{2+} for 48 h. (d-f) Viability of HCT116 and HCT116/L-OHP (d), MCF7 and MCF7/ADR (e), HCT-8 and HCT-8/TAX (f) cells treated with HPT for 48 h.

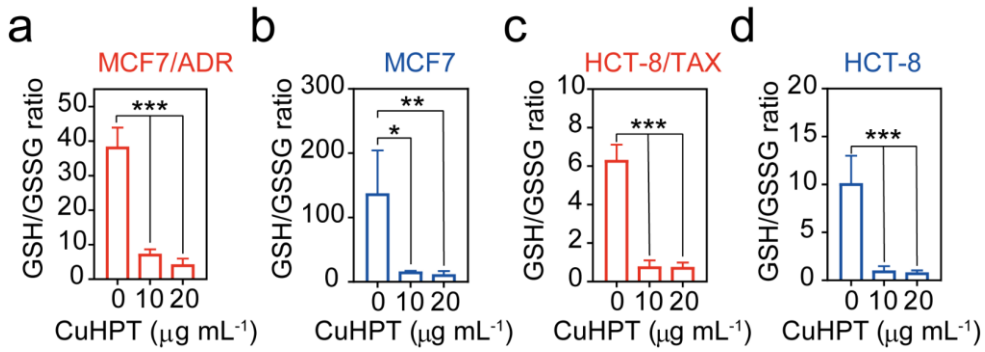

Figure S8. GSH/GSSG ratios in MCF7/ADR (a), MCF7 (b), HCT-8/TAX (c) and HCT-8 (d) cells treated with CuHPT for 24 h.

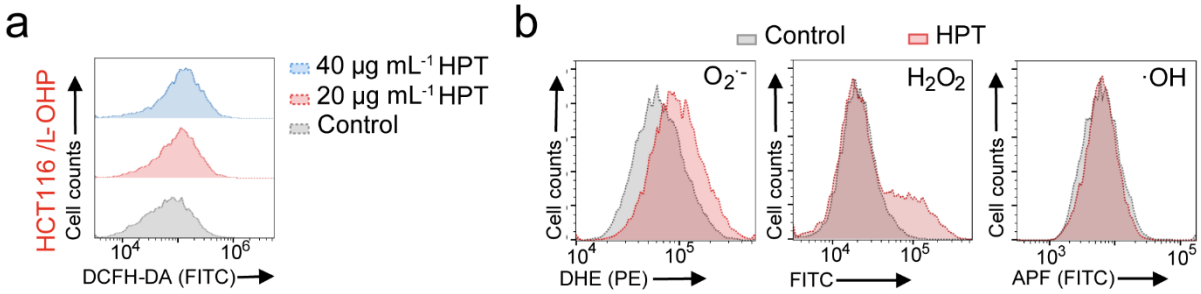

Figure S9. (a) ROS levels in HCT116/L-OHP cells treated with HPT for 24 h. (b) $O_2^{\bullet-}$, H_2O_2 and •OH levels in HCT116/L-OHP cells treated with HPT (20 μg mL^{-1}) for 24 h.

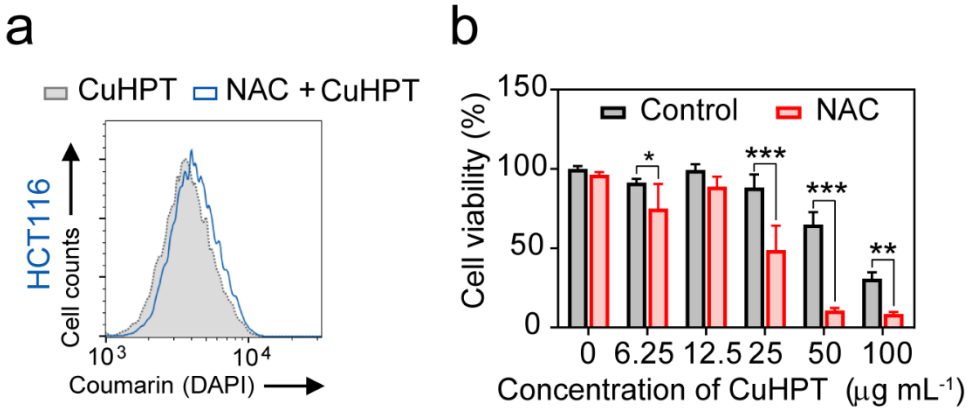

Figure S10. (a) •OH levels in HCT116 cells treated with CuHPT in the presence or absence of NAC (0.1 mM). (b) Cell viability of HCT116 cells treated with CuHPT in the presence or absence of NAC (0.4 mM).

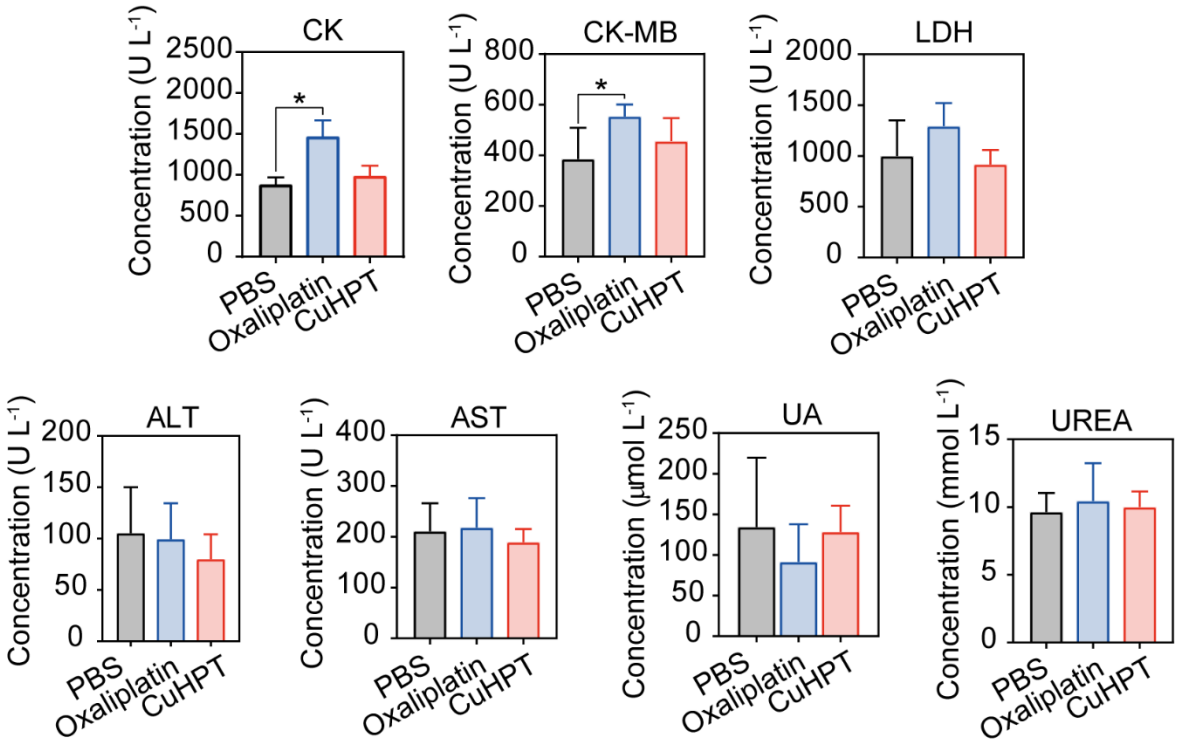

Figure S11. Serum biochemical analysis of HCT116/L-OHP tumor-bearing mice which received different treatments.

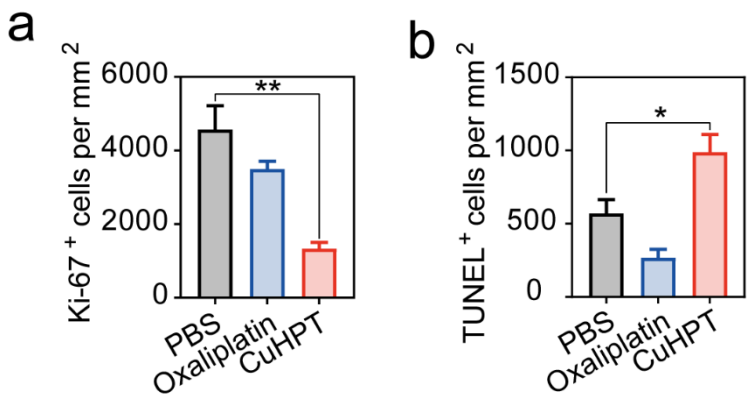

Figure S12. Statistic results of Ki-67 (a) and TUNEL (b) immunohistochemistry staining of tumors in different treatment groups.

Table S1. Comparison of CuHPT with other reported Cu-based nano-formulations for cancer therapy.

Formulations	Additional ROS generators	Cancer cells	Selectivity for drug-resistant cancer cells	References
CuHPT	No	HCT116, MCF7, HCT-8, HCT116/L-OHP, MCF7/ADR, and HCT-8/TAX	Yes	This work
Copper peroxide nanodots	No	U87MG	No	1
Cu-TBP	No	B16F10	No	2
Cu-Cys NPs	No	HeLa, MCF7, and MCF7R	No	3
Cu-HNCS	No	4T1	No	4
Cu-HCF	No	HeLa, 4T1	No	5
PGC-DOX	Glucose oxidase (GOx)	4T1	No	6
UCNPs@Cu-Cys-GOx	GOx	4T1	No	7
SC@G nanosheets	GOx	4T1	No	8
GOx@CuS	GOx	B16F10	No	9
HMON-Au-Col@Cu-TA	Au NPs (Mimetic GOx)	BxPC-3	No	10
β-lapa@Cu-PMs	β-lapachone	SMMC-7721	No	11
Cu-OCNP/Lap	β-lapachone	HeLa	No	12
Cu^{2+}-g-C_3N_4	Photodynamic therapy	HeLa	No	13
$PtCu_3$-PEG	Sonodynamic therapy	4T1	No	14
Cu-NCPs	Radiation therapy	4T1	No	15

Table S2. Comparison of CuHPT with other reported ROS-dependent nano-therapeutics for cancer therapy.

Formulations	Treatments	Exogenous antioxidants	Effects on antitumor activity	References
CuHPT	CDT	NAC, GSH-OEt	Promotion	This work
HMOS@MOF	Chemotherapy (CT)/ CDT	NAC	Inhibition	16
PEG@S-MoOx A-NRs).	Photothermal therapy (PTT)/PDT	NAC	Inhibition	17
DOX@AuHCNs-HA	PTT/PDT/CT	NAC	Inhibition	18
Fe_3O_4@PGL NP	PDT	NAC	Inhibition	19
DOX@pPt-PEG	Electrodynamic therapy (EDT)/CT	NAC	Inhibition	20
FHMP NPs	Sonodynamic therapy	NAC	Inhibition	21
Fe-Ti_3C_2	PTT/CDT	NAC	Inhibition	22
DT-PNs	CDT/CT	NAC, Vitamin C	Inhibition	23
FeMSN@PG fibres	CDT	NAC	Inhibition	24
Zr-Fc MOF	CDT/PTT	NAC	Inhibition	25
DAB NPs	CT/PTT/PDT	NAC	Inhibition	26
AgNPs	ROS and Ag ions	NAC	Inhibition	27

References

(1) Lin, L. S.; Huang, T.; Song, J.; Ou, X. Y.; Wang, Z.; Deng, H.; Tian, R.; Liu, Y.; Wang, J. F.; Liu, Y.; Yu, G.; Zhou, Z.; Wang, S.; Niu, G.; Yang, H. H.; Chen, X. Synthesis of Copper Peroxide Nanodots for H_2O_2 Self-Supplying Chemodynamic Therapy. *J. Am. Chem. Soc.* **2019**, *141* (25), 9937-9945. DOI: 10.1021/jacs.9b03457

(2) Ni, K.; Aung, T.; Li, S.; Fatuzzo, N.; Liang, X.; Lin, W. Nanoscale Metal-Organic Framework Mediates Radical Therapy to Enhance Cancer Immunotherapy. *Chem* **2019**, *5* (7), 1892-1913. DOI: 10.1016/j.chempr.2019.05.013

(3) Ma, B.; Wang, S.; Liu, F.; Zhang, S.; Duan, J.; Li, Z.; Kong, Y.; Sang, Y.; Liu, H.; Bu, W.; Li, L. Self-Assembled Copper-Amino Acid Nanoparticles for in Situ Glutathione "AND" H_2O_2 Sequentially Triggered Chemodynamic Therapy. *J. Am. Chem. Soc.* **2019**, *141* (2), 849-857. DOI: 10.1021/jacs.8b08714

(4) Lu, X.; Gao, S.; Lin, H.; Yu, L.; Han, Y.; Zhu, P.; Bao, W.; Yao, H.; Chen, Y.; Shi, J. Bioinspired Copper Single-Atom Catalysts for Tumor Parallel Catalytic Therapy. *Adv. Mater.* **2020**, *32* (36), 2002246. DOI: 10.1002/adma.202002246

(5) Wang, D.; Wu, H.; Wang, C.; Gu, L.; Chen, H.; Jana, D.; Feng, L.; Liu, J.; Wang, X.; Xu, P.; Guo, Z.; Chen, Q.; Zhao, Y. Self-Assembled Single-Site Nanozyme for Tumor-Specific Amplified Cascade Enzymatic Therapy. *Angew. Chem., Int. Ed. Engl.* **2021**, *60* (6), 3001-3007. DOI: 10.1002/anie.202008868

(6) Fu, L. H.; Wan, Y.; Qi, C.; He, J.; Li, C.; Yang, C.; Xu, H.; Lin, J.; Huang, P. Nanocatalytic Theranostics with Glutathione Depletion and Enhanced Reactive Oxygen Species Generation for Efficient Cancer Therapy. *Adv. Mater.* **2021**, *33* (7), 2006892. DOI: 10.1002/adma.202006892

(7) Wang, M.; Chang, M.; Li, C.; Chen, Q.; Hou, Z.; Xing, B.; Lin, J. Tumor-Microenvironment-Activated Reactive Oxygen Species Amplifier for Enzymatic Cascade Cancer Starvation/Chemodynamic /Immunotherapy. *Adv. Mater.* **2021**, 2106010. DOI: 10.1002/adma.202106010

(8) Yang, C.; Younis, M. R.; Zhang, J.; Qu, J.; Lin, J.; Huang, P. Programmable NIR-II

Photothermal-Enhanced Starvation-Primed Chemodynamic Therapy using Glucose Oxidase-Functionalized Ancient Pigment Nanosheets. *Small* **2020**, *16* (25), 2001518. DOI: 10.1002/smll.202001518

(9) Singh, P.; Youden, B.; Yang, Y.; Chen, Y.; Carrier, A.; Cui, S.; Oakes, K.; Servos, M.; Jiang, R.; Zhang, X. Synergistic Multimodal Cancer Therapy Using Glucose Oxidase@CuS Nanocomposites. *ACS Appl. Mater. Interfaces* **2021**, *13* (35), 41464-41472. DOI: 10.1021/acsami.1c12235

(10) Li, L.; Yang, Z.; Fan, W.; He, L.; Cui, C.; Zou, J.; Tang, W.; Jacobson, O.; Wang, Z.; Niu, G.; Hu, S.; Chen, X. In Situ Polymerized Hollow Mesoporous Organosilica Biocatalysis Nanoreactor for Enhancing ROS-Mediated Anticancer Therapy. *Adv. Funct. Mater.* **2020**, *30* (4), 1907716. DOI: 10.1002/adfm.201907716

(11) Wang, Q.; Li, X.; Mao, J.; Qin, X.; Yang, S.; Hao, J.; Guan, M.; Cao, Y.; Li, Y. Biomimic Binding Affinity Gradients Triggered GSH-Response of Core-Shell Nanoparticles for Cascade Chemo/Chemodynamic Therapy. *Adv. Healthcare Mater.* **2021**, 2101634. DOI: 10.1002/adhm.202101634

(12) He, Y.; Guo, S.; Zhang, Y.; Liu, Y.; Ju, H. NIR-II reinforced intracellular cyclic reaction to enhance chemodynamic therapy with abundant H_2O_2 supply. *Biomaterials* **2021**, *275*, 120962. DOI: 10.1016/j.biomaterials.2021.120962

(13) Ju, E.; Dong, K.; Chen, Z.; Liu, Z.; Liu, C.; Huang, Y.; Wang, Z.; Pu, F.; Ren, J.; Qu, X. Copper(II)-Graphitic Carbon Nitride Triggered Synergy: Improved ROS Generation and Reduced Glutathione Levels for Enhanced Photodynamic Therapy. *Angew. Chem., Int. Ed. Engl.* **2016**, *55* (38), 11467-11471. DOI: 10.1002/anie.201605509

(14) Zhong, X.; Wang, X.; Cheng, L.; Tang, Y. a.; Zhan, G.; Gong, F.; Zhang, R.; Hu, J.; Liu, Z.; Yang, X. GSH-Depleted $PtCu_3$ Nanocages for Chemodynamic- Enhanced Sonodynamic Cancer Therapy. *Adv. Funct. Mater.* **2019**, *30* (4), 201907954. DOI: 10.1002/adfm.201907954

(15) Wang, Y.; Ding, Y.; Yao, D.; Dong, H.; Ji, C.; Wu, J.; Hu, Y.; Yuan, A. Copper-Based Nanoscale Coordination Polymers Augmented Tumor Radioimmunotherapy for Immunogenic Cell Death Induction and T-Cell Infiltration. *Small* **2021**, *17* (8), 2006231. DOI:

10.1002/smll.202006231

(16) Ma, Y.; Su, Z.; Zhou, L.; He, L.; Hou, Z.; Zou, J.; Cai, Y.; Chang, D.; Xie, J.; Zhu, C.; Fan, W.; Chen, X.; Ju, S. Biodegradable Metal-Organic Framework-Gated Organosilica for Tumor Microenvironment-Unlocked Glutathione Depletion-Enhanced Synergistic Therapy. *Adv. Mater.* **2021**, 2107560. DOI: 10.1002/adma.202107560

(17) Wang, Y.; Gong, N.; Li, Y.; Lu, Q.; Wang, X.; Li, J. Atomic-Level Nanorings (A-NRs) Therapeutic Agent for Photoacoustic Imaging and Photothermal/Photodynamic Therapy of Cancer. *J. Am. Chem. Soc.* **2020**, *142* (4), 1735-1739. DOI: 10.1021/jacs.9b11553

(18) Xu, L.; Liu, J.; Xi, J.; Li, Q.; Chang, B.; Duan, X.; Wang, G.; Wang, S.; Wang, Z.; Wang, L. Synergized Multimodal Therapy for Safe and Effective Reversal of Cancer Multidrug Resistance Based on Low-Level Photothermal and Photodynamic Effects. *Small* **2018**, *14*, 1800785. DOI: 10.1002/smll.201800785

(19) Liang, X.; Chen, M.; Bhattarai, P.; Hameed, S.; Tang, Y.; Dai, Z. Complementing Cancer Photodynamic Therapy with Ferroptosis through Iron Oxide Loaded Porphyrin-Grafted Lipid Nanoparticles. *ACS Nano* **2021**, *15* (12), 20164-20180. DOI: 10.1021/acsnano.1c08108

(20) Chen, T.; Gu, T.; Cheng, L.; Li, X.; Han, G.; Liu, Z. Porous Pt nanoparticles loaded with doxorubicin to enable synergistic Chemo-/Electrodynamic Therapy. *Biomaterials* **2020**, *255*, 120202. DOI: 10.1016/j.biomaterials.2020.120202

(21) Huang, J.; Liu, F.; Han, X.; Zhang, L.; Hu, Z.; Jiang, Q.; Wang, Z.; Ran, H.; Wang, D.; Li, P. Nanosonosensitizers for Highly Efficient Sonodynamic Cancer Theranostics. *Theranostics* **2018**, *8* (22), 6178-6194. DOI: 10.7150/thno.29569

(22) Wu, Y.; Song, X.; Xu, W.; Sun, K. Y.; Wang, Z.; Lv, Z.; Wang, Y.; Wang, Y.; Zhong, W.; Wei, J.; Cai, H. L.; Wu, X. NIR-Activated Multimodal Photothermal/Chemodynamic/Magnetic Resonance Imaging Nanoplatform for Anticancer Therapy by Fe(II) Ions Doped MXenes (Fe-Ti_3C_2). *Small* **2021**, *17* (33), 2101705. DOI: 10.1002/smll.202101705

(23) Zhang, W.; Hu, X.; Shen, Q.; Xing, D. Mitochondria-specific drug release and reactive oxygen species burst induced by polyprodrug nanoreactors can enhance chemotherapy. *Nat.*

Commun. **2019**, *10* (1), 1704. DOI: 10.1038/s41467-019-09566-3

(24) Wang, G.; Gao, J.; Fu, Y.; Ren, Z.; Huang, J.; Li, X.; Han, G. Implantable composite fibres with Self-supplied H_2O_2 for localized chemodynamic therapy. *Chem. Eng. J.* **2020**, *388,* 124211. DOI: 10.1016/j.cej.2020.124211

(25) Deng, Z.; Fang, C.; Ma, X.; Li, X.; Zeng, Y. J.; Peng, X. One Stone Two Birds: Zr-Fc Metal-Organic Framework Nanosheet for Synergistic Photothermal and Chemodynamic Cancer Therapy. *ACS Appl. Mater. Interfaces* **2020**, *12* (18), 20321-20330. DOI: 10.1021/acsami.0c06648

(26) Chen, D.; Tang, Q.; Zou, J.; Yang, X.; Huang, W.; Zhang, Q.; Shao, J.; Dong, X. pH-Responsive PEG-Doxorubicin-Encapsulated Aza-BODIPY Nanotheranostic Agent for Imaging-Guided Synergistic Cancer Therapy. *Adv. Healthcare Mater.* **2018**, *7* (7), 1701272. DOI: 10.1002/adhm.201701272

(27) Guo, D.; Zhu, L.; Huang, Z.; Zhou, H.; Ge, Y.; Ma, W.; Wu, J.; Zhang, X.; Zhou, X.; Zhang, Y.; Zhao, Y.; Gu, N. Anti-leukemia activity of PVP-coated silver nanoparticles via generation of reactive oxygen species and release of silver ions. *Biomaterials* **2013**, *34* (32), 7884-7894. DOI: 10.1016/j.biomaterials.2013.07.015